

**Structure-sensitivity of alumina supported palladium catalysts for N<sub>2</sub>O decomposition**

Nia Richards<sup>1</sup>, James H. Carter<sup>1</sup>, Ewa Nowicka<sup>1</sup>, Luke A. Parker<sup>2</sup>, Samuel Pattisson<sup>1</sup>, Qian He<sup>1</sup>, Nicholas F. Dummer<sup>1</sup>, Stanislaw Golunski<sup>1</sup>, Graham J. Hutchings<sup>1\*</sup>

<sup>1</sup>Cardiff Catalysis Institute, School of Chemistry, Cardiff University, Cardiff, CF10 3AT UK

<sup>2</sup>Now at; Inorganic Chemistry and Catalysis Debye Institute for Nanomaterials Science, Utrecht University, Universiteitsweg 99, 3584CG Utrecht (The Netherlands)

\*Corresponding author: [Hutch@cardiff.ac.uk](mailto:Hutch@cardiff.ac.uk)

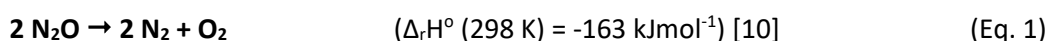
## **Abstract**

The catalytic activity of Pd/ $\gamma$ -Al<sub>2</sub>O<sub>3</sub> for N<sub>2</sub>O decomposition was found to be highly dependent on the preparation methodology and the number of reaction cycles. Chloride species on the surface of a 2.6 wt. % Pd-Al<sub>2</sub>O<sub>3</sub> catalyst prepared by wet impregnation were identified as inhibiting the activity. Multiple reaction cycles were shown to remove these species, and a subsequent increase in activity was observed; 10.3 mol<sub>N<sub>2</sub>O</sub> h<sup>-1</sup> kg<sub>cat</sub><sup>-1</sup> in the first use, increased to 28.7 mol<sub>N<sub>2</sub>O</sub> h<sup>-1</sup> kg<sub>cat</sub><sup>-1</sup> on the fourth use both at 550 °C. Additionally, removal of physisorbed water from the support prior to metal deposition increased the thermal stability of Pd nanoparticles and increased the catalyst activity. Catalysts were subsequently prepared using a deposition technique with an increased concentration of Cl<sup>-</sup> ions resulted in increased Pd-Cl species in the final catalyst and the catalytic activity was consequently increased due to the improved control of Pd particle size.

Keywords: Nitrous Oxide Decomposition, Particle Size, CO Chemisorption, HAADF-STEM, Pd-Al<sub>2</sub>O<sub>3</sub>.

## 1 Introduction

Nitrous oxide (N<sub>2</sub>O) is a highly potent greenhouse gas, this being evidenced by its global warming potential of *ca.* 300 relative to CO<sub>2</sub> [1–3]. 60 % of the global N<sub>2</sub>O emissions are anthropogenic and include industrial chemical processes, sewage treatment, combustion sources (both stationary and mobile) and the agricultural sector [4–7], while adipic acid production accounts for around 80 % of the global industrial emission of N<sub>2</sub>O [6,8]. There are also small industrial uses such as hospital and dental surgeries [9]. Consequently, it is of great importance to develop catalysts that can efficiently decompose N<sub>2</sub>O (Eq. 1):



There are many catalysts that can be used for N<sub>2</sub>O decomposition including perovskites [11–15], ceria-based catalysts [16–18], spinels [19–21] and supported metal catalysts [22–26]. This work focuses on palladium/alumina (Pd-Al<sub>2</sub>O<sub>3</sub>) catalysts as these have not been extensively studied to date [27–31] and similar catalytic systems have been demonstrated to exhibit high activity and stability in similar applications [32–37]. Pekridis *et al.* reported a T<sub>100</sub> (i.e. the temperature to reach 100 % conversion) of 425 °C using a 2 wt. % Pd-Al<sub>2</sub>O<sub>3</sub> catalyst prepared by wet-impregnation. They also showed that the addition of propane to the gas feed lowered the T<sub>100</sub> to 400 °C [27]. The rate-limiting step in the decomposition of N<sub>2</sub>O is typically the recombination of oxygen to form O<sub>2</sub> [38–44] and propane acts as reductant that can facilitate the abstraction of oxygen from the oxidised active site, significantly increasing the observed rate of N<sub>2</sub>O decomposition at lower temperatures [27,28]. In addition to propane [45–49] ethane, methane and CO [49–54] have also been used as reductants. Christoforou *et al.* reported that 72 % conversion was possible using 2 wt. % Pd-Al<sub>2</sub>O<sub>3</sub> at 600 °C, the addition of propane to the feed lowers the temperature required for 100 % conversion by over 200 °C. [28]. Doi *et al.* utilised a higher weight loading of 5 % with only 60 ppm N<sub>2</sub>O in the gas stream and showed that it was possible to decompose this low concentration of N<sub>2</sub>O at 300 °C; however, air was used as the balance gas of this reaction and in this case that the addition of oxygen to the feed increases the activity [31]. It is important to note that in most cases the addition of oxygen to the gas feed limits the conversion of N<sub>2</sub>O, this is because the oxygen present oxidises the active site of the catalysts [22,27,55].

A range of Pd concentrations have been shown to be active for the decomposition of N<sub>2</sub>O. Tzitzios *et al.* prepared a 0.5 wt.% Pd- Al<sub>2</sub>O<sub>3</sub> catalyst by wet impregnation using a nitrate precursor that achieved 55 % conversion of N<sub>2</sub>O at 550 °C. The group showed that the presence of a reductant (CO) to the feed lowers the temperature required for 50 % conversion (T<sub>50</sub>) from 536 °C to 366 °C, a decrease of 170 °C in the operating temperature.[56] Parres-Esclapez *et al.* also prepared a 0.5 wt.% Pd-Al<sub>2</sub>O<sub>3</sub> catalyst by

impregnation using a Pd acetate precursor that converted 34 % N<sub>2</sub>O present at 600 °C.[22] Staying on the theme of low Pd loadings, Pachatouridou *et al.* prepared a 1 wt.% Pd-Al<sub>2</sub>O<sub>3</sub> catalyst by dry impregnation, that reached 78 % conversion at 600 °C, with a T<sub>50</sub> of 525 °C.[57] Tateishi *et al.* demonstrated that a higher weight loading was also good for this reaction with a commercial 5 wt.% Pd-Al<sub>2</sub>O<sub>3</sub> catalyst achieving 100 % conversion at 320 °C, but the catalyst that the group prepared by wet impregnation required 500 °C to achieve the same conversion in the same conditions (noting O<sub>2</sub> present in gas feed) [30].

In this work, we investigate the importance of surface species and particle size of Pd-Al<sub>2</sub>O<sub>3</sub> catalysts for the decomposition of N<sub>2</sub>O in the presence and absence of a reductant, propane. The effect of removing surface species such as water and chloride ions have been investigated by different pre-treatments and support pre-treatments. In addition to comparing how activity changes based on these pre-treatments, we have evaluated how the surface sensitivity of these catalysts can be used to control the particle size and consequently, catalyst activity. Through pre-treatment of the catalyst support prior to the metal deposition, the catalytic activity is significantly increased, resulting in a decrease of the N<sub>2</sub>O T<sub>100</sub> by 150 °C to 400 °C, in the presence of propane.

## 2 Experimental

### 2.1 Catalyst Preparation

2.6 wt.% Pd-Al<sub>2</sub>O<sub>3</sub> was prepared by wet impregnation as described by Pekridis *et al.* [27], PdCl<sub>2</sub> was dissolved in deionised water to give a solution with a concentration of 6 mg mL<sup>-1</sup>. γ-Al<sub>2</sub>O<sub>3</sub> (0.98 g, Sigma Aldrich, average particle size < 50 nm) was then added to the solution (4.6 mL) and heated slowly to 55 °C with stirring to remove the water via evaporation until a slurry was formed. The slurry was then dried in an oven at (120 °C, 2 h) and calcined (600 °C, 4 h, heating rate 10 °C min<sup>-1</sup> in flowing air). Where stated further heat treatments were carried out at 600 °C for 1 h at 20 °C min<sup>-1</sup> in flowing air. In some cases γ-Al<sub>2</sub>O<sub>3</sub> was calcined before catalyst preparation at 600 °C for 4 h at 10 °C min<sup>-1</sup> in flowing compressed dry air. The following denominations were assigned to various catalysts: **SC** – Support calcined at 600 °C for 4 h at 10 °C min<sup>-1</sup> in flowing compressed dry air before catalyst preparation. **5HT** – catalyst prepared, calcined and subjected to 5 more heat treatments at 600 °C for 1 h at 20 °C min<sup>-1</sup> in flowing compressed dry air. **4R** – catalyst that has been through four reaction cycles. **5R** – catalyst that has been through five reaction cycles.

2.1 wt.% Pd-Al<sub>2</sub>O<sub>3</sub> was prepared by a modified impregnation method as described by Morad and co-workers [58]. PdCl<sub>2</sub> was dissolved in water to give a solution with a concentration of 6 mg mL<sup>-1</sup>, HCl was added to acidify the solution until a concentration of 0.58 M was achieved. De-ionised water was added to the solution (3.49 mL) to a total volume of 16 mL in a 50 mL round bottom flask. The solution was heated to 60 °C in an oil bath. γ-Al<sub>2</sub>O<sub>3</sub> (0.98 g, Sigma Aldrich, average particle size < 50 nm) was added to the solution slowly over a period of 10 min. The slurry was left to stir for 15 min and then the temperature was increased to 95 °C and left to dry for 16 h. The resulting solid was calcined at 600 °C for 4 h at 10 °C min<sup>-1</sup> in flowing compressed dry air. As with the wet impregnation samples, one catalyst was prepared with γ-Al<sub>2</sub>O<sub>3</sub> that had been calcined before catalyst preparation at 600 °C for 4 h at 10 °C min<sup>-1</sup> in flowing compressed dry air and was also denoted support calcined (**MI SC**). The catalyst that was prepared by modified impregnation using untreated Al<sub>2</sub>O<sub>3</sub> was denoted **MI**.

### 2.2 N<sub>2</sub>O decomposition studies

All reactions were performed at atmospheric pressure in a continuous-flow fixed-bed reactor. A reactor tube (4.6 mm internal diameter, stainless steel) was packed with catalyst (0.0625 g) between two layers of quartz wool. Reactions were performed over the temperature range of 200 – 600 °C, with a flow rate of 100 ml/min (GHSV 76690 h<sup>-1</sup>). The gas feed was composed of 1 % N<sub>2</sub>O in He or 1 % N<sub>2</sub>O and 1 % C<sub>3</sub>H<sub>8</sub> in He. All outgoing gaseous products were analysed online using an Agilent 7890B Gas Chromatograph (GC) (columns: Hayesep Q (80-100 mesh, 1.8 m) MolSieve 5A (80-100 mesh, 2 m)

fitted with a thermal conductivity detector. Pre-treatment of the  $\gamma$ - $\text{Al}_2\text{O}_3$  in the reactor prior to the addition of the metal was carried out using 13 %  $\text{O}_2$  and 87 %  $\text{N}_2$  from separate cylinders (BOC grade N4, 99.99 %).

### 2.3 Catalyst Characterisation

X-ray photoelectron spectroscopy (XPS) was performed on a Thermo Fisher Scientific K-alpha<sup>+</sup> spectrometer. Samples were analysed using a micro-focused monochromatic Al X-ray source (72 W) over an area of approximately 400 microns. Data was recorded at pass energies of 150 eV for survey scans and 40 eV for high resolution scan with 1 eV and 0.1 eV step sizes respectively. Charge neutralisation of the sample was achieved using a combination of both low energy electrons and argon ions. Data analysis was performed in CasaXPS using a Shirley type background and Scofield cross sections, with an energy dependence of -0.6.

Solid-state Magic Angle Spinning Nuclear Magnetic Resonance (MAS-NMR) spectra were obtained at the EPSRC UK National Solid-state NMR Service Durham University. Solid state  $^1\text{H}$  Proton spectra were recorded at 399.88 MHz using a Varian VNMRs spectrometer and a 4 mm (rotor o.d.) magic-angle spinning probe. They were obtained using a background suppression pulse sequence, 128 repetitions with a 1 s recycle delay and a spin-rate of approximately 14 kHz. Spectral referencing was to external, neat tetramethylsilane carried out by setting the resonance from adamantane to 1.9 ppm.

Powder X-Ray Diffraction (XRD) analysis was performed on a PANalytical X'Pert Pro diffractometer using a Ni-filtered  $\text{CuK}\alpha$  radiation source operating at 40 KV and 40 mA. Standard analysis was performed using a 40 minute run with a back filled sample holder. Patterns were identified using the International Center for Diffraction Data Powder Diffraction File.

*In-situ* XRD was performed using a PANalytical X'Pert Pro diffractometer using a Ni-filtered  $\text{CuK}\alpha$  radiation source operating at 40 KV and 40 mA, fitted with a cell that allows temperature control and gas flow using Bronkhorst MFC's. 'Data collector' program controls temperature settings, run time and repeats. Patterns were identified using the International Center for Diffraction Data Powder Diffraction File.

High-Angle Annular Dark-Field Scanning Transmission Electron Microscopy (HAADF-STEM) was performed using a JEOL ARM 200CF AC-STEM instrument and the samples were prepared using the dry dispersion route: The catalyst powder was ground between two clean glass slides and then dry transferred onto a holey carbon TEM grid.

136 Inductively Coupled Plasma – Optical Emission Spectroscopy (ICP-OES) was performed by Exeter  
137 Analytical Services using HF digestion to get an accurate Pd loading. The sample was digested by Anton  
138 Paar Multiwave 3000 microwave with nitric and HF acids – then the HF was neutralised with the  
139 addition of Boric Acid. A reagent blank was carried out. Internal standard was added to the resulting  
140 solutions and the blank and sample were run against Fe standards by ICP-OES using Thermo Fisher  
141 iCAP Duo 7400.

142 CO Chemisorption was performed using a ChemBET TPR/TPD pulsar with a reduction in 10 % H<sub>2</sub>/Ar up  
143 to 150 °C before carrying out CO chemisorption at room temperature using 10 % CO/He using an  
144 attenuation of 2, TCD sensitivity of 150 and CO flow of 15 mL min<sup>-1</sup>. An automated pulse program was  
145 used with a pulse length of 400 seconds, loop volume 125 µL, 16 pulses and a stable baseline.

Pd-Al<sub>2</sub>O<sub>3</sub> catalysts have previously been shown to catalyse N<sub>2</sub>O decomposition at high reaction temperatures (>500 °C) [22,27,30,56,57]. Initially, their stability was investigated through the use of multiple reaction cycles. The catalyst was heated step wise from 200 – 600 °C in 50 °C increments under a mixture of N<sub>2</sub>O (1 %) in helium and the N<sub>2</sub>O conversion was recorded every 50 °C. Following this, the catalyst bed was cooled under flowing helium and the reaction process repeated. In each cycle, the catalyst was exposed to the same pre-treatment as the initial test, as described in the experimental section. The catalytic activity could then be compared across the reaction cycles and differences investigated through material characterisation.

Firstly, a blank reaction was performed with only quartz wool and no catalyst. No conversion of N<sub>2</sub>O was measured over the temperature range of 300 – 600 °C, indicating the reactor was not active over the temperature range of interest (Table 1, entry 1). Decomposition of N<sub>2</sub>O was studied using 2.6 wt. % Pd-Al<sub>2</sub>O<sub>3</sub> prepared by wet impregnation, with a pre-treatment (1 h at 600 °C, 13 % O<sub>2</sub>, 87 mL min<sup>-1</sup>) over the temperature range 300 – 600 °C. The fresh catalyst (Table 1 entry 2) was able to convert 10.3 mol<sub>N<sub>2</sub>O</sub> h<sup>-1</sup> kg<sub>cat</sub><sup>-1</sup> at 550 °C, while the catalyst by Tzitzious *et al.* converted 20.9 mol<sub>N<sub>2</sub>O</sub> h<sup>-1</sup> kg<sub>cat</sub><sup>-1</sup> at the same temperature.[56]

Table 1. The effect of multiple reaction cycles or heat treatments on N<sub>2</sub>O conversion over 2.6 wt. % Pd-Al<sub>2</sub>O<sub>3</sub> catalysts.

Entry	Catalyst (2.6 wt. % Pd-Al <sub>2</sub> O <sub>3</sub> )	T <sub>50</sub> <sup>a</sup> (°C)	Conversion at 550 °C (%)	Decomposition Rate at 550 °C (mol <sub>N<sub>2</sub>O</sub> h <sup>-1</sup> kg <sub>cat</sub> <sup>-1</sup> )
1	Blank	-	0	0
2	Fresh	577	24	10.3
3	2R	565	39	16.7
4	3R	542	56	24.0
5	4R	527	67	28.7
6	5R	540	57	24.4
7	5HT	584	22	9.4

<sup>a</sup> temperature required for 50 % N<sub>2</sub>O conversion;

The catalytic activity was found to increase with each reaction cycle up to the fourth use (Table 1 entries 3-5). After the second reaction cycle the decomposition rate increased from 16.7 to 24.0, this increased to a maximum at the 4<sup>th</sup> use (4R) 28.7 mol<sub>N<sub>2</sub>O</sub> h<sup>-1</sup> kg<sub>cat</sub><sup>-1</sup>. For the fifth cycle a decrease in the decomposition rate was observed to 24.4 mol<sub>N<sub>2</sub>O</sub> h<sup>-1</sup> kg<sub>cat</sub><sup>-1</sup>. The observed increase in activity after multiple uses was investigated further by replicating the five heat treatment cycles *ex situ*, i.e. in a furnace (flowing air at 600 °C for 1 h) to simulate the reaction conditions. The activity of this catalyst (denoted 5HT) did not compare to that of the multiple use catalyst, but was comparable to the fresh catalyst (Table 1, entry 7 and Fig. 1). The decomposition rate at 550 °C was 9.4 mol<sub>N<sub>2</sub>O</sub> h<sup>-1</sup> kg<sub>cat</sub><sup>-1</sup>.



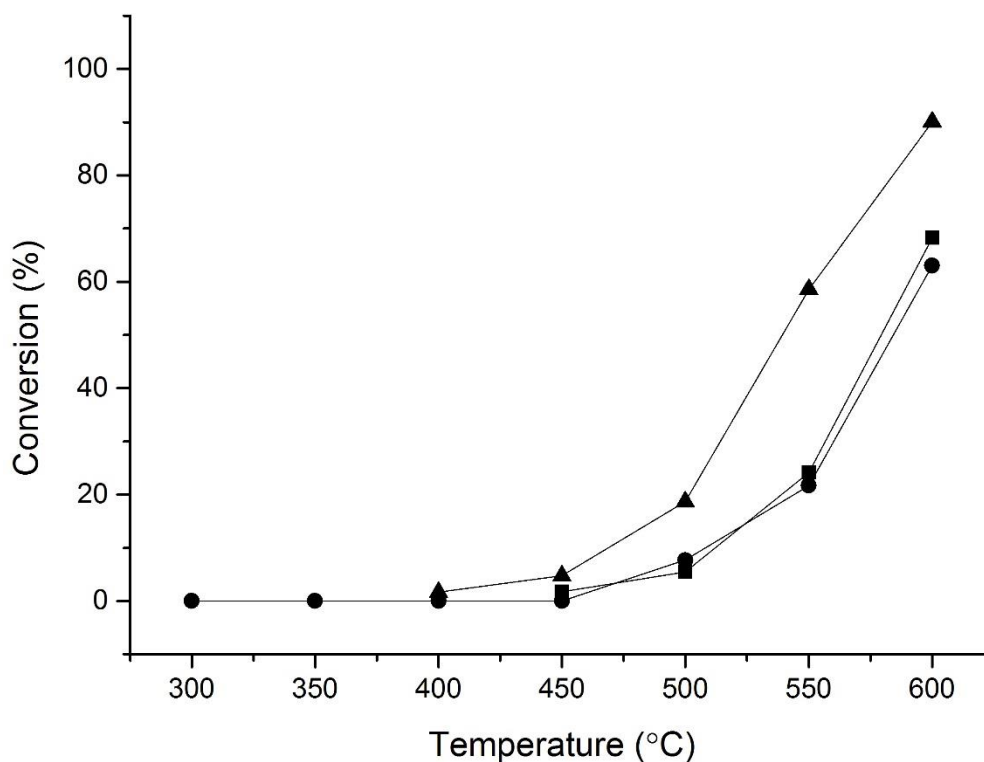


Fig. 1. The effect of multiple uses or heat treatments on N<sub>2</sub>O decomposition using a 2.6 wt. % Pd-Al<sub>2</sub>O<sub>3</sub> catalyst. Reaction Conditions: 1 % N<sub>2</sub>O/He, total flow 100 mL min<sup>-1</sup>, GHSV: 76690 h<sup>-1</sup> Legend: ■ - 2.6 wt. % Pd-Al<sub>2</sub>O<sub>3</sub> Fresh, ● - 2.6 wt. % Pd-Al<sub>2</sub>O<sub>3</sub> 5HT, ▲ - 2.6 wt. % Pd-Al<sub>2</sub>O<sub>3</sub> 5R.

The Pd-Al<sub>2</sub>O<sub>3</sub> catalysts were then characterised in an attempt to understand the origin of the activity differences observed over multiple reaction cycles and heat-treatments compared to the fresh sample. The samples of interest were the fresh 2.6 wt. % Pd-Al<sub>2</sub>O<sub>3</sub> catalyst, the catalyst after five reaction cycles (5R) and the catalyst after five heat-treatments (5HT). Fig. 2 illustrates the X-ray diffraction patterns; the support exhibits only alumina reflections, as does the fresh 2.6 wt. % Pd-Al<sub>2</sub>O<sub>3</sub> catalyst, reflection are assigned to γ-Al<sub>2</sub>O<sub>3</sub> (3 1 1) 2θ = 37.1 °, (4 0 0) 2θ = 46.0 ° and (4 4 0) 2θ = 66.6 ° [59]. There is no reflection present for Pd in the fresh catalyst, which indicates that the particle size of Pd is below the XRD nanoparticle detection limit. In contrast, the 5R and 5HT catalysts exhibited reflections due to Pd as PdO (1 0 1) 2θ = 33.855 °, PdO (3 1 1) 2θ = 54.900 ° and PdO (2 1 1) 2θ = 71.485 ° [60]. A Pd<sup>0</sup> reflection was observed at Pd (1 1 1) 2θ = 42.034 ° [61]. In the used (4R and 5R) and 5HT catalysts there are reflections present due to both PdO and Pd, this presence of reflections suggests that Pd nanoparticles have sintered as the particles are now observable by XRD.

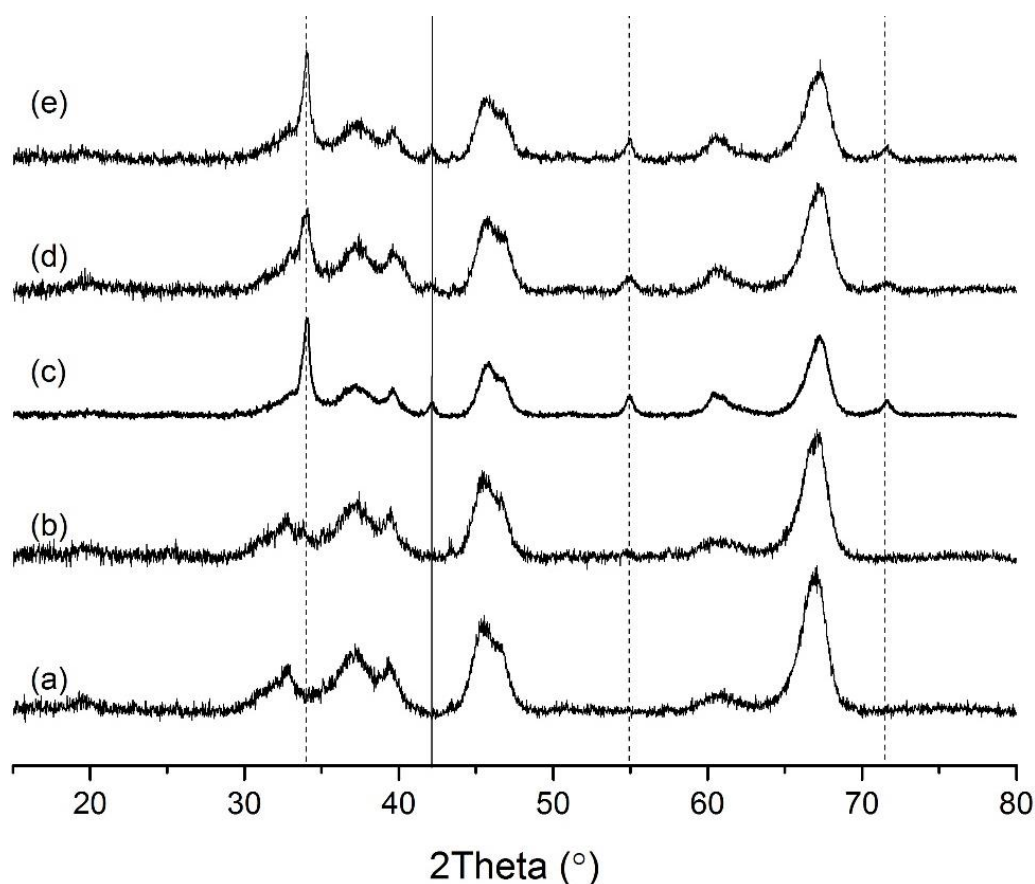


Fig. 2. XRD patterns for  $\gamma$ - $\text{Al}_2\text{O}_3$  and 2.6 wt. %  $\text{Pd-Al}_2\text{O}_3$  catalysts; (a)  $\text{Al}_2\text{O}_3$  support, (b) 2.6 wt. %  $\text{Pd-Al}_2\text{O}_3$  Fresh, (c) 2.6 wt. %  $\text{Pd-Al}_2\text{O}_3$  **4R**, (d) 2.6 wt. %  $\text{Pd-Al}_2\text{O}_3$  **5R**, (e) 2.6 wt. %  $\text{Pd-Al}_2\text{O}_3$  **5HT**, dashed line – PdO, solid line – Pd, all unlabelled reflections are due to  $\gamma$ - $\text{Al}_2\text{O}_3$ .

The improvement in activity on repeated uses may have been caused by the removal of residual Cl species that has been reported to poison the catalyst [62]. This would be achieved over the reaction cycles through a process of converting any remaining Pd-Cl species to PdO. X-Ray photoelectron spectroscopy (XPS) was used to investigate the surface composition and oxidation state of Pd in more detail (Fig. 3). In general, two peaks at 336.8 eV and 334.9 eV are observable in the Pd 3d core level XPS spectra, with the peak at 336.8 eV ascribed to PdO- $\text{Al}_2\text{O}_3$  as previously reported by Batista *et al.* [63] while the peak at 334.9 eV can be attributed to  $\text{Pd}^0$  on  $\text{Al}_2\text{O}_3$  [64,65]. Depending on catalyst preparation techniques Pd-Cl species can also be present in the spectra and correspond to the peaks at 338.2 eV [66]. Each Pd species has two peaks assigned to it due to the spin orbit splitting value of 5.3 eV [67,68]. All catalysts show only PdO and Pd-Cl species and the concentration of these species was observed to change as the catalyst was subjected to reaction conditions. Specifically, the proportion of Pd-Cl species decreased while PdO species increased, overall. The **5R** catalyst shows an increase in PdCl species over the **4R** catalysts. This is not because the catalyst has gained Cl, but because the % Pd present has decreased meaning more of the surface of the Pd is in the form PdCl as sintering has taken place. (**Error! Reference source not found.**). When the catalyst was heated in the

furnace (**5HT**) almost all the PdCl species were removed (Fig. 3), however, the catalytic activity is not improved above that of the fresh catalyst. As the number of heat treatments increases the surface concentration of total atomic Pd % (as given by XPS) decreases (Table 2), this indicates that the % of Pd at the surface has decreased, which can indicate Pd sintering or agglomeration has taken place.

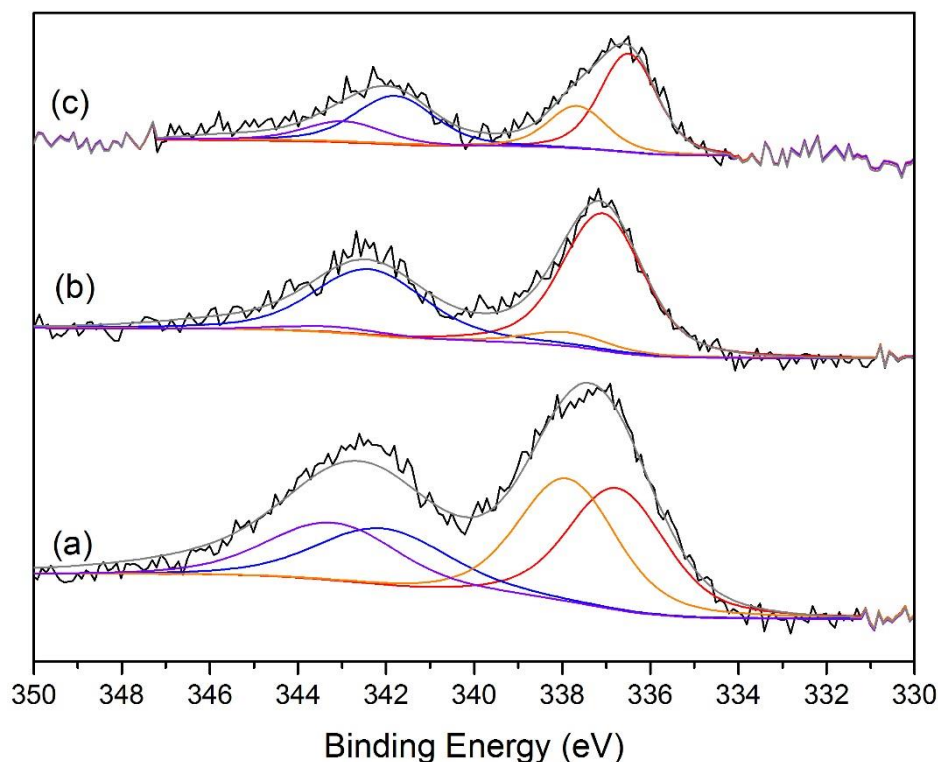


Fig. 3. XPS spectra for various 2.6 wt. % Pd-Al<sub>2</sub>O<sub>3</sub> catalysts (a) Fresh, (b) **5HT**, (c) **5R**. Each spectra is fitted with two peaks corresponding to PdO (Red and Blue lines) and Pd-Cl (Orange and Purple species).

Table 2. Surface composition of Pd-Al<sub>2</sub>O<sub>3</sub> catalysts as reported by XPS analysis.

Catalyst	Pd 3d (at.%)	% of PdO (337 eV) (%)	% of PdCl (339 eV) (%)
2.6 wt. % Pd- $\gamma$ -Al <sub>2</sub> O <sub>3</sub> Fresh	0.46	50	50
2.6 wt. % Pd- $\gamma$ -Al <sub>2</sub> O <sub>3</sub> <b>4R</b>	0.40	78	22
2.6 wt. % Pd- $\gamma$ -Al <sub>2</sub> O <sub>3</sub> <b>5R</b>	0.11	72.7	27.3
2.6 wt. % Pd- $\gamma$ -Al <sub>2</sub> O <sub>3</sub> <b>5HT</b>	0.25	92	8

The XRD patterns indicate that with increased reaction cycles and heat treatments Pd sintering took place. Furthermore, XPS measurements indicated that in addition to sintering the population of Pd-Cl species decreased across the samples. However, the N<sub>2</sub>O decomposition activity of the **4R** sample when compared to the **5HT** sample is suggestive of another factor not examinable by XPS or XRD. Therefore, HAADF-STEM was performed on the samples to provide a greater insight into the particle size changes suggested by XRD and XPS. Comparison of fresh **5R** and **5HT** 2.6 wt. % Pd-Al<sub>2</sub>O<sub>3</sub> samples

by electron microscopy are shown in Fig. 4. The fresh catalyst possesses Pd particles in the range of 1-5 nm (Fig. 4a). Large Pd particles (> 10 nm) of PdO are present after five reaction cycles (Fig. 4b), however, small particles persist. These large particles were not present in the fresh catalyst and are, therefore, consistent with analysis of the XRD and XPS results. That is PdO particles have sintered to form large nano-particles greater than 10 nm. Liu *et al.* showed that sintering is a common mechanism by which metal surface area and dispersion decreases [69,70]. In the 5HT sample, HAADF-STEM shows that there are a range of particle sizes visible with both large particles (> 5 nm) and small (< 2 nm) present. In general, the presence of the large nanoparticles indicates that during the heat treatments sintering occurred and despite the removal of Cl<sup>-</sup> ions an increase in activity was not realised, due to the concomitant the loss of metal surface area. The increase in activity of the Fresh catalyst with multiple use is due to incremental removal of Cl<sup>-</sup> ions, with a slight decrease in activity seen after the 4<sup>th</sup> cycle (**4R**) as the effect of the removal of Cl is negated by the formation of larger Pd nano-particles, as seen by HAADF-STEM in the **5R** sample. Representative particle size distributions could not be constructed due the presence of non-spherical agglomerates of nano-particles that would produce a statistically irrelevant distribution.

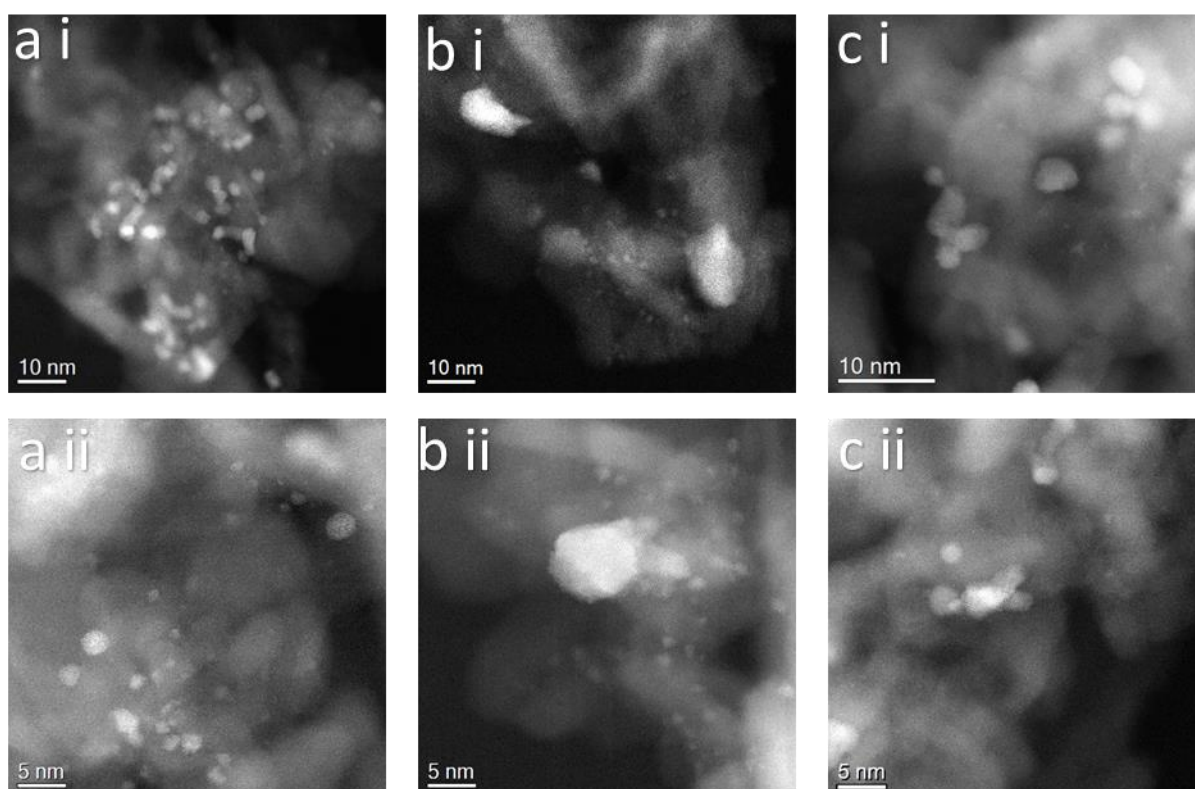


Fig. 4. HAADF-STEM images of 2.6 wt. % Pd-Al<sub>2</sub>O<sub>3</sub> Fresh (a), 5R (b), and 5 HT (c).

These initial results suggest that alongside the presence of  $\text{Cl}^-$ , the size of the Pd particles strongly contribute to the rate of  $\text{N}_2\text{O}$  decomposition. To try to achieve similar levels of activity as the catalyst which has undergone four reaction cycles a preparatory method to control Pd particle sizes was explored. This would negate the need to carry out multiple catalyst test cycles. As  $\text{Al}_2\text{O}_3$  is hygroscopic, it was hypothesised that the removal of surface water species and carbonates (the C 1s region of the XPS spectra showed peak at 289.7 eV, that is indicative of  $\text{O}-\text{C}=\text{O}$ , carbonate species) could enhance the dispersion of Pd, as these species may block the pore structure of the support [71,72]. Therefore, the alumina support was calcined under flowing air at 600 °C at 10 °C  $\text{min}^{-1}$  for 4 h before metal deposition (denoted as **SC**) and a 2.6 wt. % Pd- $\text{Al}_2\text{O}_3$  catalyst was then prepared by wet impregnation. Analysis of the calcined alumina supported the inference of water removal from the surface through calcination, as illustrated by solid state magic angle spinning (MAS)  $^1\text{H}$  NMR (Fig. 5).

The properties of the untreated, as-received  $\text{Al}_2\text{O}_3$  and calcined  $\text{Al}_2\text{O}_3$  were investigated by NMR (Fig. 5**Error! Reference source not found.**). Both spectra contain a single broad peak that is associated to the protons of physisorbed water. The difference in broadness is related to the quantity of water absorbed on the surface of the support. The spectra suggest that there are more physisorbed water molecules present on the untreated sample compared to that of the calcined sample. Both spectra reveal a significant resonance at 4.6 ppm that corresponds to hydrogen bonded water on the  $\text{Al}_2\text{O}_3$  surface. Spectra of the untreated sample has a shoulder present that is not present in the calcined sample, this shoulder at 1.2 ppm is due to the presence of non-hydrogen bonded physisorbed water [73,74]. In this spectra there is also a slight shoulder at 7 ppm; this resonance is due to Brønsted acid sites that are produced when water adsorbs onto a Lewis acidic site [75]. The absence of these two shoulder resonances indicates that water was removed during the calcination treatment.

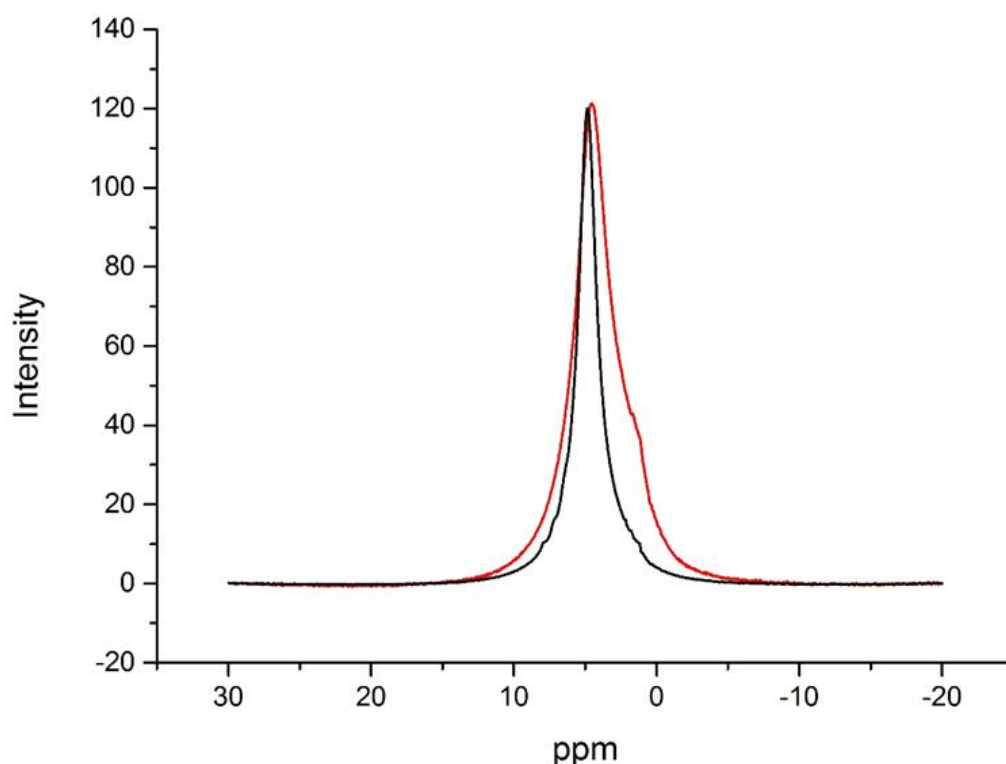


Fig. 5. Solid-state  $^1\text{H}$  NMR spectrum of  $\text{Al}_2\text{O}_3$  Fresh (red) and calcined (black)

Furthermore, calcination of the support led to a change in the point of zero charge (PZC) of the  $\gamma\text{-Al}_2\text{O}_3$ , from  $\text{PZC} = 8.43$  for the untreated support, to 8.04 after calcination (see supplementary information Fig. S1 and Fig. S2). The measured pH of the  $\text{PdCl}_2$  solution used to prepare the catalysts was 1.0, and the Pd solution was confirmed to comprise of  $\text{PdCl}_3(\text{H}_2\text{O})^-$  by Raman spectroscopy (see supplementary information Fig. S3). When the pH of the solution is lower than that of the PZC, the surface will be protonated and will strongly interact with anions [76,77] therefore the decrease in PZC of the calcined catalyst will mean the surface is less positively-charged during the catalyst preparation. This modification in surface charge may be beneficial for the dispersion of the Pd nanoparticles on the support, as is the case for the preparation of gold catalysts by deposition-precipitation.[78] Therefore the 2 wt. % Pd- $\text{Al}_2\text{O}_3$  **SC** would be expected to have a better dispersion than the palladium supported on the untreated support. An accurate Pd weight loading on both the fresh and **SC** Pd- $\text{Al}_2\text{O}_3$  catalysts was performed with ICP-OES, both catalysts had a 2.61 wt. % Pd loading.

HAADF-STEM shows that similar Pd nanostructures are present in the fresh and **SC** catalysts with nanoparticles and clusters present in both samples (Fig. 6). However, HAADF-STEM indicates that in the **SC** catalyst there are an increased quantity of small nanoparticles than in the fresh catalyst (Fig. 6b). The HAADF-STEM of the **SC** catalyst featured many nanoparticles less than 1 nm and some nanoparticles in the range of 3 – 8 nm. When compared to the **5R** catalyst which has undergone multiple reaction cycles there are significantly more smaller nanoparticles present in the **SC** catalyst

(Fig. 6b). For the **5R** sample (Fig. 4b) there are no nanoparticles that are sub 1 nm, whereas these are easily identifiable in the SC catalyst (Fig. 6b).

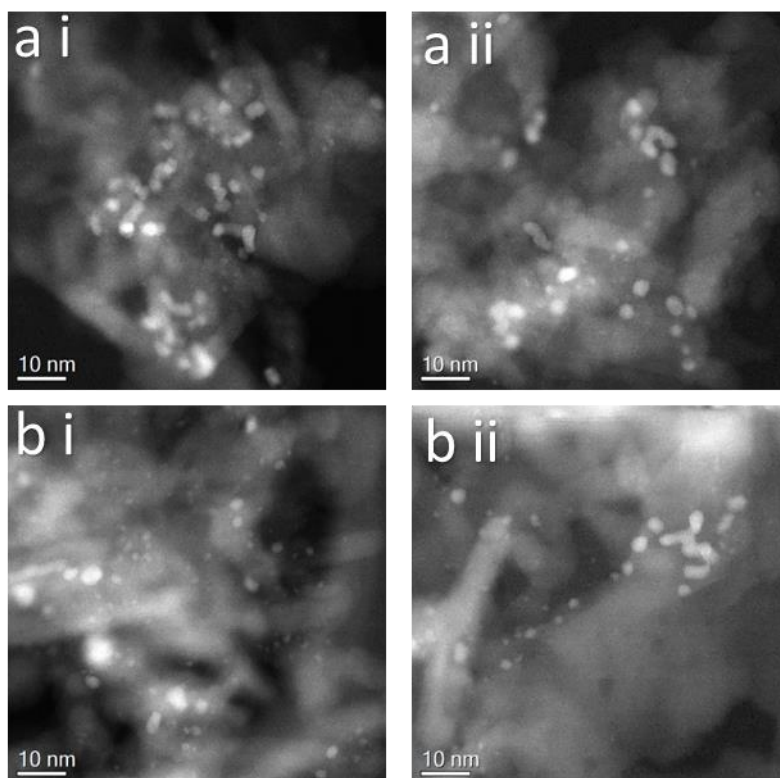


Fig. 6. HADDF-STEM images of 2.6 wt. % Pd-Al<sub>2</sub>O<sub>3</sub> Fresh (a) and Support calcined (**SC**) (b)

The SC catalyst was evaluated for N<sub>2</sub>O decomposition and compared to the fresh and **5R** catalysts (Fig. 7). The T<sub>50</sub> obtained over the **SC** catalyst was found to be 561 °C and compared to the values of 577 and 540 °C over the fresh and **5R** catalysts. Therefore, the support pre-treatment step has increased the N<sub>2</sub>O decomposition rate to 15.9 mol<sub>N<sub>2</sub>O</sub> h<sup>-1</sup> kg<sub>cat</sub><sup>-1</sup> at 550 °C and is indicative of the formation of a higher density of active Pd nano-particles. Performing, a comparable reaction cycle with the **SC** catalyst resulted in a modest increase of the decomposition rate to 18.8 mol<sub>N<sub>2</sub>O</sub> h<sup>-1</sup> kg<sub>cat</sub><sup>-1</sup> at 550 °C and a decrease of the T<sub>50</sub> to 556 °C over the fifth use catalyst (**SC 5R**). We consider the modest improvement in the decomposition rate suggests that the PdCl population has decreased as with the **5R** sample.

It has been shown previously that adding a reductant (such as propane [45–49]) to the gas feed lowers the temperature required for 100 % conversion. This is due to the rate limiting step of N<sub>2</sub>O decomposition being the desorption and recombination of oxygen to form O<sub>2</sub> [38–44]. Propane acts as reductant that can facilitate the abstraction of oxygen from the oxidised active site, significantly increasing the observed rate of N<sub>2</sub>O decomposition at lower temperatures [27,28]. In this case the



presence of propane lowers the temperature required by almost 200 °C. Reactions were carried out with the addition of propane in the gas feed (1 %). The dramatic increase in decomposition activity is observed with all catalysts but is most noticeable with the **SC** catalyst, as with N<sub>2</sub>O only, 95 % conversion is achieved at 600 °C, in the presence of propane 95 % conversion is achieved at 350 °C.

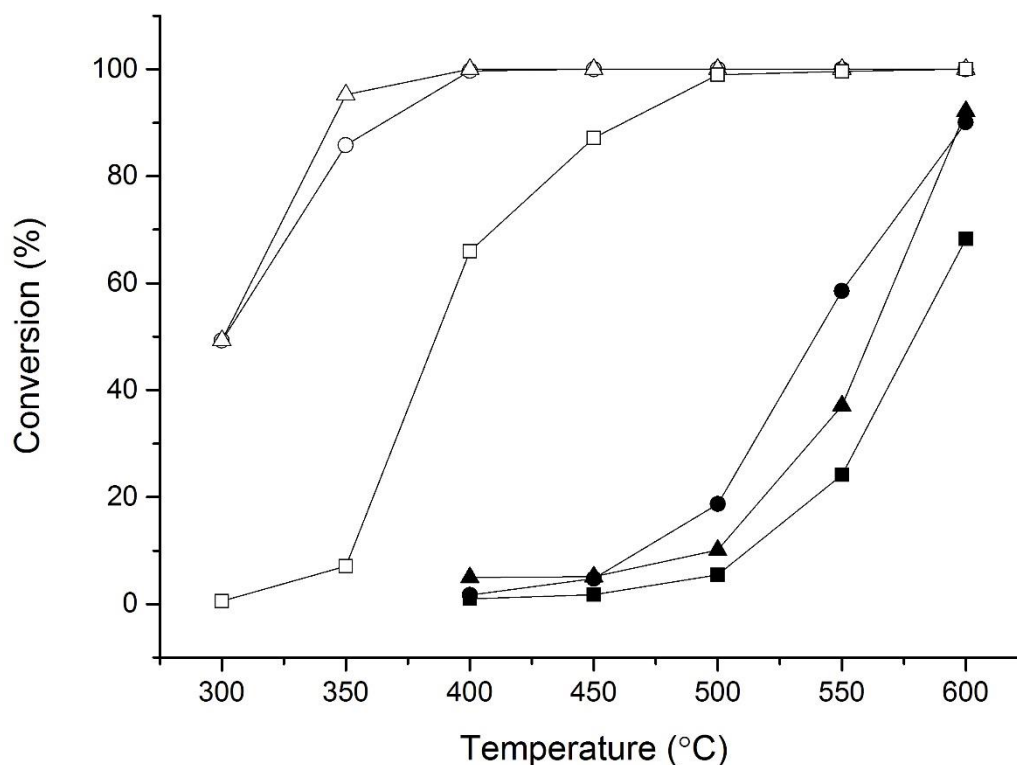


Fig. 7. The effect on N<sub>2</sub>O conversion of heat treatments on 2.6 wt. % Pd-Al<sub>2</sub>O<sub>3</sub>. Reaction Conditions: total flow 100 mL min<sup>-1</sup>, GHSV: 76690 h<sup>-1</sup>, 300 - 600 °C, Closed symbols: 1 % N<sub>2</sub>O/He, Open symbols: 1 % N<sub>2</sub>O/1 % C<sub>3</sub>H<sub>8</sub>/He. Legend: ■ - 2.6 wt. % Pd-Al<sub>2</sub>O<sub>3</sub> Fresh, ● - 2.6 wt. % Pd-Al<sub>2</sub>O<sub>3</sub> 5R, ▲ - 2.6 wt. % Pd-Al<sub>2</sub>O<sub>3</sub> SC.

The superior dispersion Pd on the **SC** catalyst, as evidenced by HAADF-STEM implies that the anchoring of Pd is stronger on the calcined support. To examine directly the stability of the Pd species on the surface of the Al<sub>2</sub>O<sub>3</sub>, *in situ* XRD was performed. The *in situ* XRD profiles of 2.6 wt. % Pd-Al<sub>2</sub>O<sub>3</sub> and **SC** catalysts are illustrated in Fig. 8a and b, respectively. The samples were heated in 1 % N<sub>2</sub>O/N<sub>2</sub> and cooled in N<sub>2</sub> at 50 °C intervals. The *in situ* XRD patterns of 2.6 wt. % Pd-Al<sub>2</sub>O<sub>3</sub> shows that small PdO reflections were present at 500 °C, with the intensity of the PdO reflections not increasing past 550 °C, with Pd<sup>0</sup> reflections forming at the same temperatures. In the **SC** catalyst PdO and Pd reflections were not visible until at least 600 °C. The difference in temperature required to observe reflections corresponding to nanoparticles of PdO and Pd indicates that the Pd nanoparticles are more strongly anchored to the calcined Al<sub>2</sub>O<sub>3</sub> than the untreated support. The effect of the reaction time-on-line was investigated, (Fig. S4), and the fresh catalyst sharply loses activity over the first 3 h, before following



a downward trend over the next 15 h. This catalyst is not stable during long term reactions. However, the **SC** catalyst shows promise, initially there is a decrease in activity in the first hour but the activity then improves, and the catalyst is stable over an 18 h period with the conversion of N<sub>2</sub>O remaining constant. These observation are in agreement with the *in situ* XRD data.

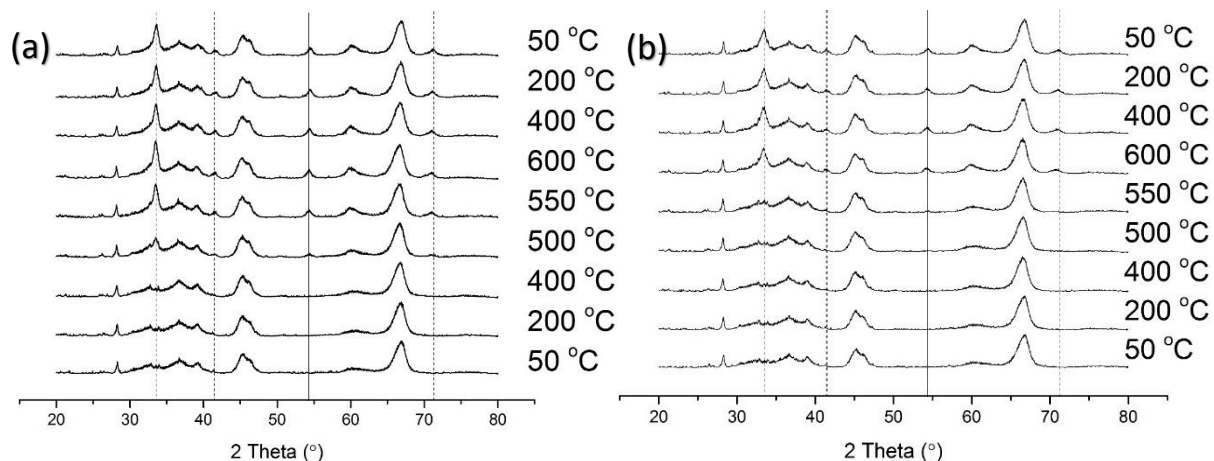


Fig. 8. *In situ* XRD patterns taken at regular temperature intervals for (a) 2.6 wt. % Pd-Al<sub>2</sub>O<sub>3</sub> Fresh and (b) 2.6 wt. % Pd-Al<sub>2</sub>O<sub>3</sub> **SC** heated in 1 % N<sub>2</sub>O/N<sub>2</sub> and then cooled in N<sub>2</sub>. Solid Line; Pd, Dashed line; PdO.

The average particle size of the Pd present on the surface was further investigated with CO chemisorption of the fresh and **SC** catalysts. It is assumed that all Pd particles are hemispherical and that one CO molecule will bind to one Pd atom, STEM has shown this is not the case but this will give an average particle size and metal surface area. Metal nanoparticle dispersion increased modestly from 24.7 % to 27.5 % with the fresh to the **SC** catalyst (Table 3). The average particle size of Pd particles in the **SC** catalyst decreased when compared to the fresh catalyst. This decrease in average particle size indicated that the nanoparticles found on the **SC** catalyst are smaller and further support the inference that smaller particles are more active than larger particles for N<sub>2</sub>O decomposition. This is due to the smaller particles having a larger surface area per gram of metal and this small change in particle size facilitates an increased decomposition reaction rate through the increased surface area available.

Table 3. Dispersion and metal surface area as calculated by CO Chemisorption on 2.6 wt. % Pd-Al<sub>2</sub>O<sub>3</sub> fresh and SC.

Catalyst	Metal Surface Area (m <sup>2</sup> g <sup>-1</sup> )	Avg. particle size (nm)	Dispersion (%)
2.6 wt. % Pd-Al <sub>2</sub> O <sub>3</sub> Fresh	2.9	1.51	24.7
2.6 wt. % Pd-Al <sub>2</sub> O <sub>3</sub> <b>SC</b>	3.2	1.36	27.5

The catalytic activity for N<sub>2</sub>O decomposition when propane is present with the fresh and **SC** catalysts is markedly different (Fig. 7). To investigate the effect of particle size, the catalysts were re-prepared using a modified impregnation (**MI**) technique which has been shown previously to produce catalysts with a very narrow particle size distribution [58]. Palladium was deposited with the MI technique on a calcined alumina and an as-received alumina and examined by XPS, XRD, CO chemisorption and HAADF-STEM. The Pd loading of the MI prepared catalysts was analysed by ICP-OES and was found to be lower (2.1 wt.%) than the traditionally prepared impregnation catalysts (2.6 wt. %). The materials were examined by CO chemisorption (Table 4) and this revealed that the average Pd particle size, 1.25 and 1.28 nm was smaller than the analogue impregnation catalysts displayed in Table 3. However, the metal surface area was found to be lower and can be assigned to the lower Pd loading of the **MI** catalysts. When comparing the XRD patterns of 2.1 wt. % Pd-Al<sub>2</sub>O<sub>3</sub> **MI** catalysts, it is clear that there are no Pd or PdO reflections (see supplementary information Fig. S5). This indicates that the Pd species are smaller than the detection limit of XRD, which is consistent with the CO chemisorption data.

Table 4. Dispersion and metal surface area as calculated by CO Chemisorption on 2.1 wt. % Pd-Al<sub>2</sub>O<sub>3</sub> fresh and **SC** prepared by modified impregnation.

Catalyst	Metal Surface Area (m <sup>2</sup> g <sup>-1</sup> )	Avg. particle size (nm)	Dispersion (%)
2.1 wt.% Pd-Al <sub>2</sub> O <sub>3</sub> Fresh <b>MI</b>	2.8	1.25	29.8
2.1 wt.% Pd-Al <sub>2</sub> O <sub>3</sub> <b>SC MI</b>	2.7	1.28	29.3

The modified impregnation technique requires an excess of HCl to be added during the preparation. This facilitates the deposition of Pd and the subsequently observed metal particle control, through altering the support PZC and inducing an increased interaction between the Pd precursor and the support. Characterisation by XPS shows a high ratio of PdO to PdCl in the modified impregnation catalysts. For both the un-calcined supported catalyst (2.1 wt. % Pd-Al<sub>2</sub>O<sub>3</sub> Fresh **MI**) and the calcined supported catalyst (2.1 wt. % Pd-Al<sub>2</sub>O<sub>3</sub> **SC MI**), there is an elevated population of Pd-Cl species compared to PdO species, despite undergoing calcination (Fig. 9**Error! Reference source not found.**

and Table 5). In contrast, when comparing the ratio of PdO to PdCl species for the 2.6 wt. % Pd-Al<sub>2</sub>O<sub>3</sub> **SC** catalyst was found to have more PdO present than PdCl.

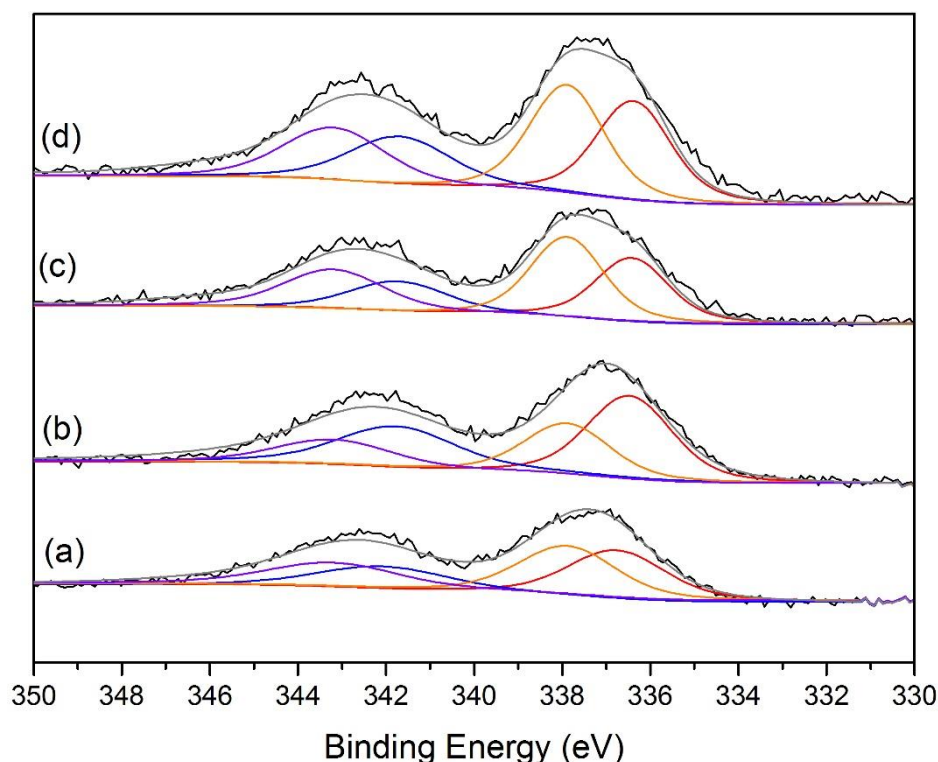


Fig. 9. XPS spectra for fresh or SC Pd-Al<sub>2</sub>O<sub>3</sub> catalysts prepared by impregnation (2.6 wt. % Pd) or Modified Impregnation (2.1 wt. % Pd). Legend: (a) Fresh, (b) **SC**, (c) **MI**, (d) **MI SC**. Each spectra is fitted with two peaks corresponding to PdO and PdCl species. Legend: Red and Blue – PdO, Orange and Purple – PdCl.

Table 5. Surface composition of Pd- Al<sub>2</sub>O<sub>3</sub> catalysts as reported by XPS analysis

Catalyst	Pd 3d (at.%)	% of PdO (337 eV) (%)	% of PdCl (339 eV) (%)
2.6 wt. % Pd-Al <sub>2</sub> O <sub>3</sub> <b>SC</b>	0.48	62.3	37.7
2.1 wt. % Pd-Al <sub>2</sub> O <sub>3</sub> Fresh <b>MI</b>	0.39	43.5	56.5
2.1 wt. % Pd-Al <sub>2</sub> O <sub>3</sub> SC <b>MI</b>	0.42	47.6	52.3

The 2.1 wt.% Pd/Al<sub>2</sub>O<sub>3</sub> **MI** and 2.1 wt.% Pd/Al<sub>2</sub>O<sub>3</sub> **SC MI** catalysts were tested for N<sub>2</sub>O decomposition with and without propane present and compared to the equivalent impregnation catalysts (Fig. 10.a and b). When only N<sub>2</sub>O is present in the gas feed there is still minor difference in activity, with the **SC MI** catalyst modestly outperforming, that of the fresh **MI** catalyst (Fig. 10.a). The **MI** catalysts outperform the corresponding impregnation catalysts, and further support the supposition that the N<sub>2</sub>O decomposition reaction is sensitive to the active surface composition and structure. This reactivity can be attributed to the increased dispersion of smaller and more active metal particles available for

N<sub>2</sub>O decomposition to occur, based on the results from CO Chemisorption (Table 4). However, the increased Cl<sup>-</sup> on the surface of the **MI** catalysts restricts the activity to only the minor improvement observed. The T<sub>50</sub> obtained over the **MI** catalyst was found to be 576 °C and compared to the values of 547 °C over the **MI SC** catalyst. Therefore, the support pre-treatment step has increased the N<sub>2</sub>O decomposition rate from 16.3 mol<sub>N<sub>2</sub>O</sub> h<sup>-1</sup> kg<sub>cat</sub><sup>-1</sup> to 21.9 mol<sub>N<sub>2</sub>O</sub> h<sup>-1</sup> kg<sub>cat</sub><sup>-1</sup> at 550 °C.

When propane was added to the reaction mixture the effect of calcining the support prior to Pd deposition was negated (Fig. 10b). The activity of the **MI** catalysts was lower, at ca. 78 % N<sub>2</sub>O conversion compared to that of the **SC** catalyst, but higher than that of the fresh supported Al<sub>2</sub>O<sub>3</sub> catalyst at 350 °C, compared to 96 % for **SC** and 7 % for the fresh catalyst (Fig. 10a). As the activity of both **MI** catalysts was comparable the decomposition rate was ca. 30 mol<sub>N<sub>2</sub>O</sub> h<sup>-1</sup> kg<sub>cat</sub><sup>-1</sup> at 350 °C with propane present. It is possible that residual chlorine species may inhibit the reaction as observed with the catalysts that underwent increasing reaction cycles. However, it is clear that the influence of calcining the support prior to metal impregnation is negated with the **MI** catalysts for this reaction with propane.

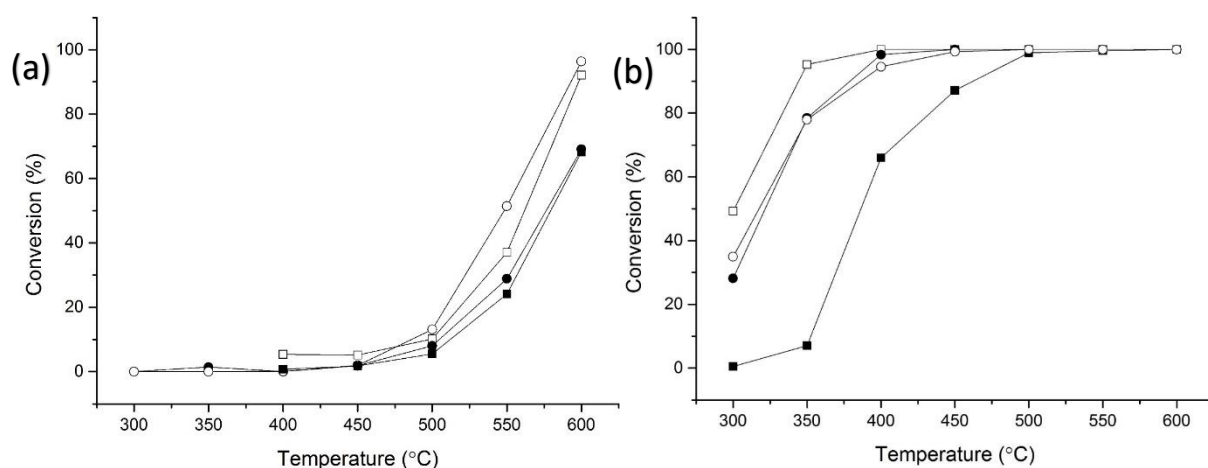


Fig. 10. The effect on N<sub>2</sub>O conversion of catalyst preparation over Pd-Al<sub>2</sub>O<sub>3</sub> Fresh (filled symbols) and **SC** catalysts (open symbols): ■ - 2.6 wt.% Pd Fresh, □ - 2.6 wt.% Pd SC, ● - 2.1 wt.% Pd **MI**, ○ - 2.1 wt.% Pd **SC MI**. Reaction conditions; (a), 1 % N<sub>2</sub>O/He, total flow 100 ml min<sup>-1</sup>, GHSV: 75900 h<sup>-1</sup>, (b), 1 % N<sub>2</sub>O/1 % C<sub>3</sub>H<sub>8</sub>/He, total flow 100 ml min<sup>-1</sup>, GHSV: 75900 h<sup>-1</sup>.

HAADF-STEM images of the fresh **MI** catalyst (Fig. 11a) and the post-reaction **MI** catalyst (Fig. 11b) show small, uniform particles that sinter after multiple uses. The particles that are present on the fresh **MI** catalyst are sub 2 nm, with only a few particles larger than 2 nm. After one reaction cycle, some of the particles present were measured to be ca. 5 nm, indicating that Pd sintering has taken place. We consider that although the modified impregnation technique does provide increased control over the metal nano-particle size it does not control the metal-support interaction. In theory,

the modified impregnation solution is more acidic due to the presence of HCl so the surface of the support is more positively charged. The consequence of this should be a stronger interaction between the precursor and the support, resulting in an increased metal dispersion compared to a conventional impregnation technique. However, as the support is not calcined it can be hypothesised that the interaction between the smaller particles produced by MI and the support may not be sufficiently strong due to the presence of water and can diminish the strength at which the Pd can anchor to the support and consequently lead to sintering.

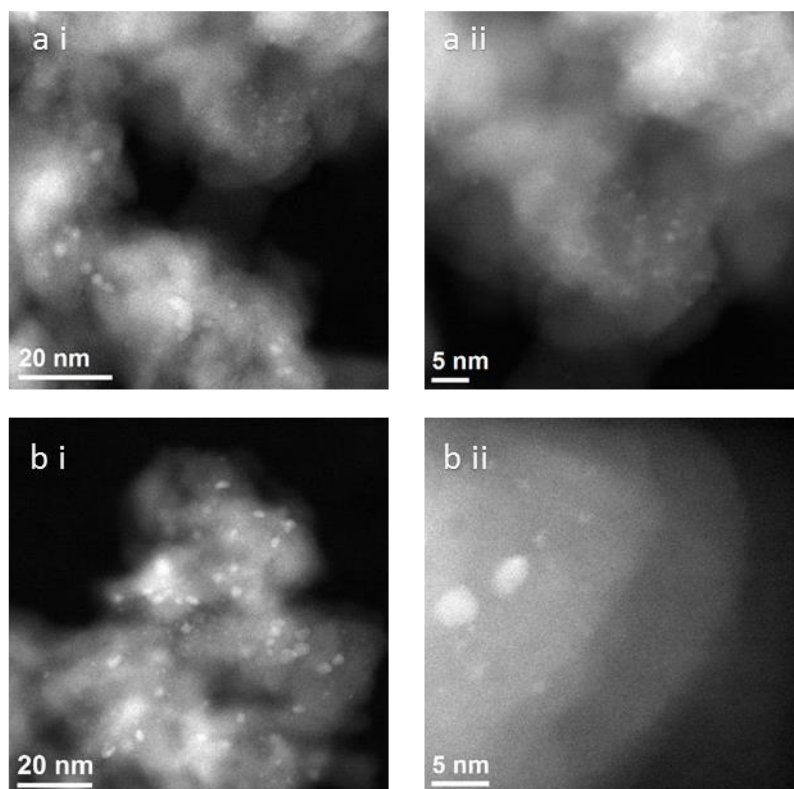


Fig. 11. HAADF-STEM images of 2.1 wt. % Pd-Al<sub>2</sub>O<sub>3</sub> **MI** (a) **MI** fresh, (b) catalyst following one reaction cycle (**MI 1R**).

Table 6. Comparison of the key catalysts in this manuscript with literature examples.

Catalyst	T <sub>50</sub> <sup>a</sup> (°C)	Conversion at 550 °C (%)	Decomposition Rate at 550 °C (mol <sub>N<sub>2</sub>O</sub> h <sup>-1</sup> kg <sub>cat</sub> <sup>-1</sup> )	T <sub>100</sub> <sup>b</sup> in the presence of propane (°C)	Ref
Blank	-	0	0	-	This work
2.6 wt. % Pd- Al <sub>2</sub> O <sub>3</sub> <b>Fresh</b>	577	24	10.3	550	This work
2.6 wt. % Pd- Al <sub>2</sub> O <sub>3</sub> <b>4R</b>	527	67	28.7	-	This work
2.6 wt. % Pd- Al <sub>2</sub> O <sub>3</sub> <b>5R</b>	540	57	24.4	400	This work

2.6 wt. % Pd- Al <sub>2</sub> O <sub>3</sub> <b>5HT</b>	584	22	9.4	450	This work
2.6 wt. % Pd- Al <sub>2</sub> O <sub>3</sub> <b>SC</b>	562	37	15.9	400	This work
2.1 wt. % Pd- Al <sub>2</sub> O <sub>3</sub> <b>MI</b>	576	29	12.42	450	This work
2.1 wt. % Pd- Al <sub>2</sub> O <sub>3</sub> <b>MI SC</b>	548	52	22.3	450	This work
2 wt. % Pd- Al <sub>2</sub> O <sub>3</sub>	350	100	2.6	400	Pekridis [27]
0.5 wt. % Pd- Al <sub>2</sub> O <sub>3</sub>	536	52	20.9	-	Tzitzios [56]
1 wt. % Pd- Al <sub>2</sub> O <sub>3</sub>	525	59	23.7	-	Pachatouridou [57]

<sup>a</sup> the temperature at 50 % N<sub>2</sub>O conversion; <sup>b</sup> the temperature at 100 % N<sub>2</sub>O conversion in the presence of propane.

428

429 The reactivity data (Table 6) highlights the structural sensitivity of the active site and how important  
430 the relationship between Pd dispersion and presence of PdCl is. The increase in Pd dispersion resulted  
431 in an increase in activity as seen when the support is calcined before catalyst preparation. However,  
432 removal of Cl<sup>-</sup> from the catalyst surface as with the catalysts that have undergone four or five reaction  
433 cycles can lead to an improvement in activity despite the onset of Pd sintering and reduced Pd  
434 dispersion. Further activity gains can be observed through careful control of the Pd dispersion, through  
435 the MI technique despite a high density of PdCl. Therefore, the balance between a high Pd dispersion  
436 and the presence of PdCl appears to favour the former. For comparison the previous literature data  
437 are included in Table 6, and these demonstrate that the catalyst preparation conditions are key to  
438 designing an active catalyst.

439

## 4 Conclusions

---

The effect of heat treatment conditions on a 2.6 wt. % Pd-Al<sub>2</sub>O<sub>3</sub> catalysts have been investigated for the catalytic decomposition of N<sub>2</sub>O into N<sub>2</sub> and O<sub>2</sub> in the absence and presence of a reducing agent (C<sub>3</sub>H<sub>8</sub>). It was found that the use of several reaction cycles increases the conversion of N<sub>2</sub>O from 24 % to 57 % at 600 °C. These multiple use catalysts also show improved stability on-stream. It has also been demonstrated that by calcining the support before catalyst preparation, similar conversions as the multiple use catalyst can be achieved in the first cycle of the **SC** catalyst. This procedure enables the high activity to be achieved on the initial use rather than on the 5<sup>th</sup> cycle (**5R**). We consider that this is due to the removal of water species lowering the PZC of the support, which suggests a reduced interaction between the Pd ion and the support surface, leading to the formation of smaller nanoparticles. When a reductant is present the temperature at which *ca.* 100 % conversion is observed is decrease from 550 °C to 350 °C. The presence of the reductant enhances the decomposition of N<sub>2</sub>O to N<sub>2</sub>, however a limited amount of O<sub>2</sub> is measured, suggesting that the reductant was acting as a scavenger of oxygen to form cracked, oxidation products and water. When the support was calcined before catalyst preparation, the resultant catalyst was formed of small Pd nanoparticles. Reaction data indicate that small nanoparticles are the more active species, as when the particle size is controlled by using a modified impregnation preparation method the activity of both catalysts is the same, therefore further supporting the hypothesis that the particle size and subsequently the metal dispersion control the activity of a Pd-Al<sub>2</sub>O<sub>3</sub> catalysts for N<sub>2</sub>O decomposition.

## 5 Acknowledgements

---

ERC Funding 'After the GoldRush' code, ERC-AtG-291319. We would like to thank Exeter Analytical for the ICP-OES data, Durham University for Solid state NMR, Oakridge National Laboratory for HAADF-STEM images and the Catalysis Hub for use of the ChemBET pulsar machine.

- [1] J. Pérez-Ramírez, F. Kapteijn, K. Schöffel, J.A. Moulijn, Formation and control of N<sub>2</sub>O in nitric acid production: Where do we stand today?, *Appl. Catal. B Environ.* 44 (2003) 117–151. doi:10.1016/S0926-3373(03)00026-2.
- [2] J. Weimann, Toxicity of nitrous oxide., *Best Pract. Res. Clin. Anaesthesiol.* 17 (2003) 47–61. <http://www.ncbi.nlm.nih.gov/pubmed/12751548>.
- [3] P. Grace, L. Barton, <http://theconversation.com/meet-n2o-the-greenhouse-gas-300-times-worse-than-co2-35204>, <Http://Theconversation.Com/Meet-N2o-the-Greenhouse-Gas-300-Times-Worse-than-Co2-35204>. (n.d.) 2015-10–29.
- [4] Intergovernmental Panel on Climate Change, Climate Change 2007 Synthesis Report, 2008. doi:10.1256/004316502320517344.
- [5] L. Li, J. Xu, J. Hu, J. Han, Reducing nitrous oxide emissions to mitigate climate change and protect the ozone layer, *Environ. Sci. Technol.* 48 (2014) 5290–5297. doi:10.1021/es404728s.
- [6] Intergovernmental Panel on Climate Change, Climate Change 2013: The Physical Science Basis. Contribution of Working Group I to the Fifth Assessment Report of the Intergovernmental Panel on Climate Change, 2013. doi:10.1017/CBO9781107415324.
- [7] M. Jabłońska, R. Palkovits, It is no laughing matter: Nitrous oxide formation in diesel engines and advances in its abatement over rhodium-based catalysts, *Catal. Sci. Technol.* 6 (2016) 7671–7687. doi:10.1039/c6cy01126h.
- [8] UNEP, Drawing Down Nitrous Oxide To Protect Climate and the Ozone Layer, 2013. doi:10.13140/2.1.4720.8646.
- [9] S.S. Maroufi, M.J. Gharavi, M. Behnam, A. Samadikuchaksaraei, Nitrous oxide levels in operating and recovery rooms of Iranian hospitals, *Iran. J. Public Health.* 40 (2011) 75–79.
- [10] F. Kapteijn, J. Rodriguez-Mirasol, J.A. Moulijn, Heterogeneous catalytic decomposition of nitrous oxide, *Appl. Catal. B Environ.* 9 (1996) 25–64. doi:10.1016/0926-3373(96)90072-7.
- [11] S. Kumar, Y. Teraoka, A.G. Joshi, S. Rayalu, N. Labhsetwar, Ag promoted La<sub>0.8</sub>Ba<sub>0.2</sub>MnO<sub>3</sub> type perovskite catalyst for N<sub>2</sub>O decomposition in the presence of O<sub>2</sub>, NO and H<sub>2</sub>O, *J. Mol. Catal. A Chem.* 348 (2011) 42–54. doi:10.1016/j.molcata.2011.07.017.
- [12] S. Kumar, A. Vinu, J. Subrt, S. Bakardjieva, S. Rayalu, Y. Teraoka, N. Labhsetwar, Catalytic N<sub>2</sub>O decomposition on Pr<sub>0.8</sub>Ba<sub>0.2</sub>MnO<sub>3</sub> type perovskite catalyst for industrial emission control, *Catal. Today.* 198 (2012) 125–132. doi:10.1016/j.cattod.2012.06.015.
- [13] J.P. Dacquin, C. Lancelot, C. Dujardin, P. Da Costa, G. Djega-Mariadassou, P. Beaunier, S. Kaliaguine, S. Vaudreuil, S. Royer, P. Granger, Influence of preparation methods of LaCoO<sub>3</sub> on the catalytic performances in the decomposition of N<sub>2</sub>O, *Appl. Catal. B Environ.* 91 (2009) 596–604. doi:10.1016/j.apcatb.2009.06.032.
- [14] K.K. Kartha, M.R. Pai, A.M. Banerjee, R. V. Pai, S.S. Meena, S.R. Bharadwaj, Modified surface and bulk properties of Fe-substituted lanthanum titanates enhances catalytic activity for CO + N<sub>2</sub>O reaction, *J. Mol. Catal. A Chem.* 335 (2011) 158–168. doi:10.1016/j.molcata.2010.11.028.
- [15] N. Russo, D. Mescia, D. Fino, G. Saracco, V. Specchia, N<sub>2</sub>O decomposition over perovskite catalysts, *Ind. Eng. Chem. Res.* 46 (2007) 4226–4231. doi:10.1021/ie0612008.
- [16] M. Zabilskiy, B. Erjavec, P. Djinić, A. Pintar, Ordered mesoporous CuO-CeO<sub>2</sub> mixed oxides as



504 an effective catalyst for N<sub>2</sub>O decomposition, *Chem. Eng. J.* 254 (2014) 153–162.  
505 doi:10.1016/j.cej.2014.05.127.

506 [17] H. Zhou, P. Hu, Z. Huang, F. Qin, W. Shen, H. Xu, Preparation of NiCe mixed oxides for catalytic  
507 decomposition of N<sub>2</sub>O, *Ind. Eng. Chem. Res.* 52 (2013) 4504–4509. doi:10.1021/ie400242p.

508 [18] H. Zhou, Z. Huang, C. Sun, F. Qin, D. Xiong, W. Shen, H. Xu, Catalytic decomposition of N<sub>2</sub>O over  
509 Cu<sub>x</sub>Ce<sub>1-x</sub>O mixed oxides, *Appl. Catal. B Environ.* 125 (2012) 492–498.  
510 doi:10.1016/j.apcatb.2012.06.021.

511 [19] B.M. Abu-Zied, S.A. Soliman, S.E. Abdellah, Enhanced direct N<sub>2</sub>O decomposition over Cu<sub>x</sub>Co<sub>1-x</sub>  
512 Co<sub>2</sub>O<sub>4</sub> (0.0 ≤ x ≤ 1.0) spinel-oxide catalysts, *J. Ind. Eng. Chem.* 21 (2015) 814–821.  
513 doi:10.1016/j.jiec.2014.04.017.

514 [20] P. Stelmachowski, G. Maniak, J. Kaczmarczyk, F. Zasada, W. Piskorz, A. Kotarba, Z. Sojka, Mg  
515 and Al substituted cobalt spinels as catalysts for low temperature deN<sub>2</sub>O-Evidence for  
516 octahedral cobalt active sites, *Appl. Catal. B Environ.* 146 (2014) 105–111.  
517 doi:10.1016/j.apcatb.2013.05.027.

518 [21] R. Amrousse, A. Tsutsumi, A. Bachar, D. Lahcene, N<sub>2</sub>O catalytic decomposition over nano-sized  
519 particles of Co-substituted Fe<sub>3</sub>O<sub>4</sub> substrates, *Appl. Catal. A Gen.* 450 (2013) 253–260.  
520 doi:10.1016/j.apcata.2012.10.036.

521 [22] S. Parres-Esclapez, M.J. Illan-Gomez, C.S.M. de Lecea, A. Bueno-Lopez, On the importance of  
522 the catalyst redox properties in the N<sub>2</sub>O decomposition over alumina and ceria supported Rh,  
523 Pd and Pt, *Appl. Catal. B Environ.* 96 (2010) 370–378. doi:10.1016/j.apcatb.2010.02.034.

524 [23] K. Yuzaki, T. Yarimizu, S. Ito, K. Kunimori, Catalytic decomposition of N<sub>2</sub>O over supported  
525 rhodium catalysts: high activities of Rh/USY and Rh/Al<sub>2</sub>O<sub>3</sub> and the effect of Rh precursors,  
526 *Catal. Letters.* 47 (1997) 173–175.  
527 <http://link.springer.com/article/10.1023/A:1019017407609>.

528 [24] F. Kapteijn, G. Mul, G. Marbán, J. Rodriguez-Mirasol, J.A. Moulijn, Decomposition of nitrous  
529 oxide over ZSM-5 catalysts, in: 11th Int. Congr. Catal. - 40th Anniv. Vol. 101, 1996: pp. 641–  
530 650. doi:10.1016/S0167-2991(96)80275-8.

531 [25] C. Kordulis, H. Latsios, A. Lycourghiotis, P. Pomonis, Kinetics of N<sub>2</sub>O Decomposition on Fe-3+  
532 Supported on Pure and Li-Modified Al<sub>2</sub>O<sub>3</sub>, *Int. J. Chem. Tech. Res.* 88 (2015) 201–205.  
533 doi:10.1016/j.physe.2016.11.016.

534 [26] Y. Li, J.N. Armor, Catalytic decomposition of nitrous oxide on metal exchanged zeolites, *Applied*  
535 *Catal. B, Environ.* 1 (1992) 1–9. doi:10.1016/0926-3373(92)80019-V.

536 [27] G. Pekridis, C. Athanasiou, M. Konsolakis, I. V. Yentekakis, G.E. Marnellos, N<sub>2</sub>O abatement over  
537 gamma-Al<sub>2</sub>O<sub>3</sub> supported catalysts: Effect of reducing agent and active phase nature, *Top.*  
538 *Catal.* 52 (2009) 1880–1887. doi:10.1007/s11244-009-9346-6.

539 [28] S.C. Christoforou, E.A. Efthimiadis, I.A. Vasalos, Catalytic conversion of N<sub>2</sub>O to N<sub>2</sub> over metal-  
540 based catalysts in the presence of hydrocarbons and oxygen, *Catal. Letters.* 79 (2002) 137–147.

541 [29] M. Machida, T. Watanabe, S. Ikeda, T. Kijima, A dual-bed lean deNO<sub>x</sub> catalyst system consisting  
542 of NO-H<sub>2</sub>-O<sub>2</sub> reaction and subsequent N<sub>2</sub>O decomposition, *Catal. Commun.* 3 (2002) 233–  
543 238. doi:10.1016/S1566-7367(02)00091-2.

544 [30] Y. Tateishi, T. Tsuneyuki, H. Furukawa, S. Kagawa, I. Moriguchi, Y. Kanmura, Y. Teraoka,  
545 Investigation on catalysts for the direct decomposition of nitrous oxide for waste anesthetic  
546 gas purification, *Catal. Today.* 139 (2008) 59–63. doi:10.1016/j.cattod.2008.08.008.

- 547 [31] K. Doi, Y.Y. Wu, R. Takeda, A. Matsunami, N. Arai, T. Tagawa, S. Goto, Catalytic decomposition  
548 of N<sub>2</sub>O in medical operating rooms over Rh/Al<sub>2</sub>O<sub>3</sub>, Pd/Al<sub>2</sub>O<sub>3</sub>, and Pt/Al<sub>2</sub>O<sub>3</sub>, Appl. Catal. B  
549 Environ. 35 (2001) 43–51. doi:10.1016/S0926-3373(01)00231-4.
- 550 [32] K. Zorn, S. Giorgio, E. Halwax, C.R. Henry, H. Gronbeck, G. Rupprechter, CO Oxidation on  
551 Technological Pd - Al<sub>2</sub>O<sub>3</sub> Catalysts : Oxidation State and Activity, J. Phys. Chem. C. 115 (2011)  
552 1103–1111. doi:10.1021/jp106235x.
- 553 [33] T. Maillet, C. Solleau, J. Barbier, D. Duprez, Oxidation of carbon monoxide, propene, propane  
554 and methane over a Pd/Al<sub>2</sub>O<sub>3</sub> catalyst. Effect of the chemical state of Pd, Appl. Catal. B Environ.  
555 14 (1997) 85–95. doi:10.1016/S0926-3373(97)00014-3.
- 556 [34] A.S. Ivanova, E.M. Slavinskaya, R. V. Gulyaev, V.I. Zaikovskii, O.A. Stonkus, I.G. Danilova, L.M.  
557 Plyasova, I.A. Polukhina, A.I. Boronin, Metal-support interactions in Pt/Al<sub>2</sub>O<sub>3</sub> and  
558 Pd/Al<sub>2</sub>O<sub>3</sub> catalysts for CO oxidation, Appl. Catal. B Environ. 97 (2010) 57–71.  
559 doi:10.1016/j.apcatb.2010.03.024.
- 560 [35] D. Roth, P. Gélin, A. Kaddouri, E. Garbowski, M. Primet, E. Tena, Oxidation behaviour and  
561 catalytic properties of Pd/Al<sub>2</sub>O<sub>3</sub> catalysts in the total oxidation of methane, Catal. Today. 112  
562 (2006) 134–138. doi:10.1016/j.cattod.2005.11.048.
- 563 [36] D. Gao, C. Zhang, S. Wang, Z. Yuan, S. Wang, Catalytic activity of Pd/Al<sub>2</sub>O<sub>3</sub> toward the  
564 combustion of methane, Catal. Commun. 9 (2008) 2583–2587.  
565 doi:10.1016/j.catcom.2008.07.014.
- 566 [37] J. Lu, B. Fu, M.C. Kung, G. Xiao, J.W. Elam, H.H. Kung, P.C. Stair, Coking- and Sintering-Resistant  
567 Palladium Catalysts Achieved Through Atomic Layer Deposition, Science. 335 (2012) 1205–  
568 1208. doi:10.1126/science.1212906.
- 569 [38] H. Guesmi, D. Berthomieu, L. Kiwi-Minsker, Nitrous Oxide Decomposition on the Binuclear [Fe  
570 II (μ-O)(μ-OH)Fe II ] Center in Fe-ZSM-5 Zeolite, J. Phys. Chem. C. 112 (2008) 20319–20328.  
571 doi:10.1021/jp808044r.
- 572 [39] C. Sang, B.H. Kim, C.R.F. Lund, Effect of NO upon N<sub>2</sub>O Decomposition over Fe/ZSM-5 with Low  
573 Iron Loading<sup>†</sup>, J. Phys. Chem. B. 109 (2005) 2295–2301. doi:10.1021/jp048884m.
- 574 [40] N. Hansen, A. Heyden, A.T. Bell, F.J. Keil, A Reaction Mechanism for the Nitrous Oxide  
575 Decomposition on Binuclear Oxygen Bridged Iron Sites in {Fe-ZSM-5}, J. Phys. Chem. C. 111  
576 (2007) 2092–2101. doi:10.1021/jp065574q.
- 577 [41] D.A. Bulushev, L. Kiwi-minsker, A. Renken, Dynamics of N<sub>2</sub>O decomposition over Fe / ZSM-5  
578 catalysts : effects of, Ind. Eng. Chem. Res. 211 (2004) 2004.
- 579 [42] K. Sun, H. Xia, E. Hensen, R. van Santen, C. Li, Chemistry of N<sub>2</sub>O Decomposition on active sites  
580 with different nature: Effect of high temperature treatment of Fe/ZSM-5, J. Catal. 238 (2006)  
581 186–195. doi:10.1016/j.jcat.2005.12.013.
- 582 [43] G.D. Pirngruber, The surface chemistry of N<sub>2</sub>O decomposition on iron containing zeolites (I), J.  
583 Catal. 219 (2003) 456–463. doi:10.1016/S0021-9517(03)00220-3.
- 584 [44] B. R. Wood, J.A. Reimer, A.T. Bell, Studies of N<sub>2</sub>O Adsorption and Decomposition on Fe–ZSM-5,  
585 J. Catal. 209 (2002) 151–158. doi:10.1006/jcat.2002.3610.
- 586 [45] H. Ohtsuka, T. Tabata, O. Okada, L.M.F. Sabatino, G. Bellussi, A study on selective reduction of  
587 NO<sub>x</sub> by propane on Co-Beta, Catal. Letters. 44 (1997) 265–270.
- 588 [46] H. Ohtsuka, T. Tabata, O. Okada, L.M.. Sabatino, G. Bellussi, A study on the roles of cobalt  
589 species in NO<sub>x</sub> reduction by propane on Co-Beta, Catal. Today. 42 (1998) 45–50.

doi:10.1016/S0920-5861(98)00075-3.

[47] R.W. Van Den Brink, S. Booneveld, M.J.F.M. Verhaak, F.A. De Bruijn, Selective catalytic reduction of N<sub>2</sub>O and NO<sub>x</sub> in a single reactor in the nitric acid industry, *Catal. Today*. 75 (2002) 227–232. doi:10.1016/S0920-5861(02)00073-1.

[48] G. Centi, F. Vazzana, Selective Catalytic Reduction of N<sub>2</sub>O in Industrial Emissions Containing O<sub>2</sub>, H<sub>2</sub>O and SO<sub>2</sub>: Behavior of Fe/ZSM-5 Catalysts, *Catal. Today*. 53 (1999) 683–693. doi:10.1016/S0920-5861(99)00155-8.

[49] H. Abdulhamid, E. Fridell, M. Skoglundh, Influence of the Type of Reducing Agent (H<sub>2</sub>, CO, C<sub>3</sub>H<sub>6</sub> and C<sub>3</sub>H<sub>8</sub>) on the Reduction of Stored NO<sub>x</sub> in a Pt/BaO/Al<sub>2</sub>O<sub>3</sub> Model Catalyst, *Top. Catal.* 30/31 (2004) 161–168. doi:10.1023/B:TOCA.0000029745.87107.b8.

[50] G. Djéga-Mariadassou, F. Fajardie, J.F. Tempère, J.M. Manoli, O. Touret, G. Blanchard, A general model for both three-way and deNO(x) catalysis: Dissociative or associative nitric oxide adsorption, and its assisted decomposition in the presence of a reductant. Part I. Nitric oxide decomposition assisted by CO over reduced or oxidized rhodium, *J. Mol. Catal. A Chem.* 161 (2000) 179–189. doi:10.1016/S1381-1169(00)00334-4.

[51] L. He, L.C. Wang, H. Sun, J. Ni, Y. Cao, Y. He, K.N. Fan, Efficient and selective room-temperature gold-catalyzed reduction of nitro compounds with CO and H<sub>2</sub>O as the hydrogen source, *Angew. Chemie - Int. Ed.* 48 (2009) 9538–9541. doi:10.1002/anie.200904647.

[52] K. Teramura, T. Tanaka, H. Ishikawa, Y. Kohno, T. Funabiki, Photocatalytic Reduction of CO<sub>2</sub> to CO in the Presence of H<sub>2</sub> or CH<sub>4</sub> as a Reductant over MgO, *J. Phys. Chem. B*. 108 (2004) 346–354. doi:10.1021/jp0362943.

[53] K. Yogo, M. Ihara, I. Terasaki, E. Kikuchi, Selective Reduction of Nitrogen Monoxide with Methane or Ethane on Gallium Ion-exchanged ZSM-5 in Oxygen-rich Atmosphere, *Chem. Lett.* 22 (1993) 229–232. doi:10.1246/cl.1993.229.

[54] R. Burch, P.K. Loader, Investigation of Pt / & Q , and Pd / A & catalysts for the combustion of methane at low concentrations, *Appl. Catal. B Environ.* 5 (1994) 149–164.

[55] M. Konsolakis, I. V. Yentekakis, G. Pekridis, N. Kaklidis, A.C. Psarras, G.E. Marnellos, Insights into the role of SO<sub>2</sub> and H<sub>2</sub>O on the surface characteristics and de-N<sub>2</sub>O efficiency of Pd/Al<sub>2</sub>O<sub>3</sub> catalysts during N<sub>2</sub>O decomposition in the presence of CH<sub>4</sub> and O<sub>2</sub> excess, *Appl. Catal. B Environ.* 138–139 (2013) 191–198. doi:10.1016/j.apcatb.2013.02.038.

[56] V.K. Tzitzios, V. Georgakilas, Catalytic reduction of N<sub>2</sub>O over Ag-Pd/Al<sub>2</sub>O<sub>3</sub> bimetallic catalysts, *Chemosphere*. 59 (2005) 887–891. doi:10.1016/j.chemosphere.2004.11.021.

[57] E. Pachatouridou, E. Papista, E.F. Iliopoulou, A. Delimitis, G. Goula, I.V. Yentekakis, G.E. Marnellos, M. Konsolakis, Nitrous oxide decomposition over Al<sub>2</sub>O<sub>3</sub> supported noble metals (Pt, Pd, Ir): Effect of metal loading and feed composition, *J. Environ. Chem. Eng.* 3 (2015) 815–821. doi:10.1016/j.jece.2015.03.030.

[58] M. Morad, M. Sankar, E. Cao, E. Nowicka, T.E. Davies, P.J. Miedziak, D.J. Morgan, D.W. Knight, D. Bethell, A. Gavrilidis, G.J. Hutchings, Solvent-free aerobic oxidation of alcohols using supported gold palladium nanoalloys prepared by a modified impregnation method, *Catal. Sci. Technol.* 4 (2014) 3120–3128. doi:10.1039/C4CY00387J.

[59] F. Hu, X. Wu, Y. Wang, X. Lai, Ultrathin γ-Al<sub>2</sub>O<sub>3</sub> nanofibers with large specific surface area and their enhanced thermal stability by Si-doping, *RSC Adv.* 5 (2015) 54053–54058. doi:10.1039/C5RA08315J.

- 633 [60] B. Ngamsom, N. Bogdanchikova, M.A. Borja, P. Prasertthdam, Characterisations of Pd-Ag/Al<sub>2</sub>O<sub>3</sub>  
634 catalysts for selective acetylene hydrogenation: Effect of pretreatment with NO and N<sub>2</sub>O,  
635 Catal. Commun. 5 (2004) 243–248. doi:10.1016/j.catcom.2004.02.007.
- 636 [61] Y. Ning, Z. Yang, H. Zhao, Platinum recovery by palladium alloy catchment gauzes in nitric acid  
637 plants: The mechanism of platinum recovery, Platin. Met. Rev. 40 (1996) 80–87.
- 638 [62] P. Marécot, A. Fakche, B. Kellali, G. Mabilon, P. Prigent, J. Barbier, Propane and propene  
639 oxidation over platinum and palladium on alumina: Effects of chloride and water, Applied Catal.  
640 B, Environ. 3 (1994) 283–294. doi:10.1016/0926-3373(94)00003-4.
- 641 [63] J. Batista, A. Pintar, D. Mandrino, M. Jenko, V. Martin, XPS and TPR examinations of  $\gamma$ -alumina-  
642 supported Pd-Cu catalysts, Appl. Catal. A Gen. 206 (2001) 113–124. doi:10.1016/S0926-  
643 860X(00)00589-5.
- 644 [64] J.Z. Shyu, K. Otto, W.L.H. Watkins, G.W. Graham, R.K. Belitz, H.S. Gandhi, Characterization of  
645 Pd/ $\gamma$ -alumina catalysts containing ceria, J. Catal. 114 (1988) 23–33. doi:10.1016/0021-  
646 9517(88)90005-X.
- 647 [65] L. Liu, F. Zhou, L. Wang, X. Qi, F. Shi, Y. Deng, Low-temperature CO oxidation over supported  
648 Pt, Pd catalysts: Particular role of FeO<sub>x</sub> support for oxygen supply during reactions, J. Catal. 274  
649 (2010) 1–10. doi:10.1016/j.jcat.2010.05.022.
- 650 [66] A. Tressaud, S. Khairoun, H. Touhara, N. Watanabe, X-Ray Photoelectron Spectroscopy of  
651 Palladium Fluorides, Zeitschrift Anorg. Und Allg. Chemie. 540 (1986) 291–299.  
652 doi:10.1002/zaac.19865400932.
- 653 [67] J.C. Zhou, C.M. Soto, M.-S. Chen, M.A. Bruckman, M.H. Moore, E. Barry, B.R. Ratna, P.E.  
654 Pehrsson, B.R. Spies, T.S. Confer, Biotemplating rod-like viruses for the synthesis of copper  
655 nanorods and nanowires, J. Nanobiotechnol. 10 (2012) 18. doi:10.1186/1477-3155-10-18.
- 656 [68] M.C. Militello, S.J. Simko, Palladium Chloride ( PdCl<sub>2</sub> ) by XPS INSTRUMENT PARAMETERS  
657 COMMON TO ALL, Surf. Sci. 3 (1997) 402–409.
- 658 [69] R.J. Liu, P.A. Crozier, C.M. Smith, D.A. Hucul, J. Blackson, G. Salaita, Metal sintering mechanisms  
659 and regeneration of palladium/alumina hydrogenation catalysts, Appl. Catal. A Gen. 282 (2005)  
660 111–121. doi:10.1016/j.apcata.2004.12.015.
- 661 [70] J.J. Chen, E. Ruckenstein, Sintering of palladium on alumina model catalyst in a hydrogen  
662 atmosphere, J. Catal. 69 (1981) 254–273. doi:10.1016/0021-9517(81)90163-9.
- 663 [71] W. Chen, Y. Ding, X. Song, T. Wang, H. Luo, Promotion effect of support calcination on ethanol  
664 production from CO hydrogenation over Rh/Fe/Al<sub>2</sub>O<sub>3</sub> catalysts, Appl. Catal. A Gen. 407 (2011)  
665 231–237. doi:10.1016/j.apcata.2011.08.044.
- 666 [72] N. Yao, J. Chen, J. Zhang, J. Zhang, Influence of support calcination temperature on properties  
667 of Ni/TiO<sub>2</sub> for catalytic hydrogenation of o-chloronitrobenzene to o-chloroaniline, Catal.  
668 Commun. 9 (2008) 1510–1516. doi:10.1016/j.catcom.2007.12.022.
- 669 [73] C.E. Bronnimann, I. ssuer Chuang, B.L. Hawkins, G.E. Maciel, Dehydration of Silica—Aluminas  
670 Monitored by High-Resolution Solid-State Proton NMR, J. Am. Chem. Soc. 109 (1987) 1562–  
671 1564. doi:10.1021/ja00239a043.
- 672 [74] E.C. Decanio, J.C. Edwards, J.W. Bruno, Solid-State <sup>1</sup>H MAS NMR Characterization of [gamma]-  
673 Alumina and Modified [gamma]-Aluminas, J. Catal. 148 (1994) 76–83.  
674 doi:10.1006/jcat.1994.1187.
- 675 [75] M. Hunger, D. Freude, H. Pfeifer, H. Bremer, M. Jank, K.P. Wendlandt, High-resolution proton

676 magnetic resonance and catalytic studies concerning brønsted centers of amorphous Al<sub>2</sub>O<sub>3</sub>-  
677 SiO<sub>2</sub> solids, Chem. Phys. Lett. 100 (1983) 29–33. doi:10.1016/0009-2614(83)87256-X.

678 [76] J. Park, J.R. Regalbuto, A Simple, Accurate Determination of Oxide PZC and the Strong Buffering  
679 Effect of Oxide Surfaces at Incipient Wetness, J. Colloid Interf. Sci. 175 (1995) 239–252.  
680 doi:10.1006/jcis.1995.1452.

681 [77] K.P. De Jong, Synthesis of Solid Catalysts, 1st ed., Wiley-VCH Verlag GmbH & Co. KGaA, 2009.

682 [78] P. Munnik, P.E. De Jongh, K.P. De Jong, Recent Developments in the Synthesis of Supported  
683 Catalysts, Chem. Rev. 115 (2015) 6687–6718. doi:10.1021/cr500486u.

684